First demonstration of a roller-driven timestamp mechanism for long-duration observations with high time resolution using large-area emulsion films

Oda, M ; Aoki, S ; Azuma, T ; Kato, T ; Nagahara, S ; Takahashi, S ; Yamada, K ; Yamamoto, T ; Yamashita, M

(Citation)
Progress of Theoretical and Experimental Physics,2022(11):113H03

(Issue Date)
2022-11

(Resource Type)
journal article

(Version)
Version of Record

(URL)
https://hdl.handle.net/20.500.14094/0100478198

PTEP

Prog. Theor. Exp. Phys. **2022** 113H03(11 pages)
DOI: 10.1093/ptep/ptac143

First demonstration of a roller-driven timestamp mechanism for long-duration observations with high time resolution using large-area emulsion films

M. Oda, S. Aoki, T. Azuma, T. Kato, S. Nagahara, S. Takahashi, K. Yamada, T. Yamamoto, and M. Yamashita

Kobe University, Nada, Kobe 657-8501, Japan
*E-mail: oda@radix.h.kobe-u.ac.jp

Received June 4, 2022; Revised October 23, 2022; Accepted November 3, 2022; Published November 7, 2022

A multi-stage shifter allows timestamped measurements by emulsion films, which have a thin medium and high resolution ($< 1\mu$m). Using multiple layers of emulsion films that move at different speeds like hands of an analog clock, the shifter can create a unique positional displacement with respect to the time-track recorded. The time information of each track is obtained by reproducing each positional displacement by track reconstruction. We developed a new model of shifter with a lighter structure to enable a large aperture area and long-duration observation times by adding more layers. Operational testing suggested that the new shifter has a sub-second time resolution, which allows an emulsion gamma-ray telescope to obtain an imaging resolution within 1° (> 80 MeV), like previous balloon experiments. Furthermore, by adding a layer which move at 100 μm s^{-1}, it achieved the 0.1 s time resolution required for high-resolution imaging above 1 GeV. We also found the possibilities of an almost three-fold improvement in the spatial resolutions in track reconstruction compared with the conventional model and of achieving time resolution on a scale of tens of milliseconds, which would enable phase resolution of a pulsar.

Subject Index H01, H21, H22, H50

1. Introduction

Emulsion films are precise trackers that record charged particles in three dimensions with high spatial resolution($< 1\ \mu$m). The films are made by coating both sides of a plastic base with emulsion mixed with silver halide crystals. Emulsion films are vacuum-packed in a laminated sheet for light shielding and protection; stacked and/or aligned films accumulate tracks integrally until development. Each track recorded in the films is positioned and angled by an automatic readout system developed at Nagoya University [1,2]. The NETSCAN analysis method can reconstruct all tracks one by one, allowing subsequent measurement of the position displacements between films [3].

Although emulsion films originally have no time information, a multi-stage shifter [4] can give each track's arrival time with a time resolution at the one-second level. Using multiple layers of emulsion films that move at different speeds like hands of an analog clock, the shifter can create a unique positional displacement with respect to the time track recorded. Thus, after reconstruction of the tracks by NETSCAN, we can get time information of each track by reproducing each positional displacement. A multi-stage shifter has been introduced for gamma-ray observations by the Gamma Ray Astro Imager with Nuclear Emulsion (GRAINE) [5–9]

and for neutrino reaction precision measurements by the Neutrino Interaction research with Nuclear Emulsion and J-PARC Accelerator (NINJA) [10–12].

The GRAINE project aims for precise observation of cosmic gamma-rays (10 MeV–100 GeV) using a balloon-borne telescope with nuclear emulsion films. The emulsion telescope consists of a converter that detects gamma-ray events, an attitude monitor, and a multi-stage shifter. The converter consists of a stack of 100 emulsion films, which records the electrons and positrons resulting from pair-production by gamma-rays. Given the thin medium and the precise position resolution, emulsion films can record the starting point and angle of pairs produced with small multiple Coulomb scattering. This allows the determination of the incident angle with 0.1° resolution for 1 GeV gamma-rays [13] and detection of linear polarization [14], which is better than the Large Area Telescope on the Fermi Gamma-ray Space Telescope [15]. The arrival direction of gamma-rays can be determined by combining the incident angle with information from the attitude monitor via the arrival time given by the multi-stage shifter.

The attitude change of the telescope in the balloon experiment is ∼0.3 degree s^{-1} without controls. The attitude monitor continuously takes star images, so the multi-stage shifter needs to have sub-second time resolution to obtain an imaging resolution within 1°. In addition, a 0.1 s time resolution would allow 0.1° imaging resolution, and a millisecond time resolution would allow phase-resolved analysis of pulsars: e.g., phase-resolved polarization measurements.

The multi-stage shifter has been operated in three balloon experiments and has obtained sub-second time resolution in the 2018 balloon experiment, which realized the highest-resolution imaging of the Vela pulsar (> 80 MeV). Although future emulsion experiments will attempt to obtain large statistics with a large-area telescope, the conventional shifter becomes too heavy with large aperture areas. We developed a new model of shifter with a lighter structure to enable a large aperture area. This paper describes the research and development of a new multi-stage shifter for introduction to future experiments, including the next experiment in 2023.

2. Multi-stage shifter

2.1 *Conventional model*

The multi-stage shifters used in various experiments were stage-driven models (Fig. 1). This model has emulsion films mounted on a metal stage, which is driven following metal guide rails. The first multi-stage shifter has an aperture area of 125 cm^2, mass of 4.7 kg, and consists of three drive stages. It was operated in a balloon experiment in 2011 [5,6] and accelerator neutrino experiments in 2014–2015 [10,11]. The second multi-stage shifter has an aperture area of 0.38 m^2, weighs 65 kg, and consists of a fixed stage and three drive stages. It was operated in the 2015 and 2018 balloon experiments [7–9] and the 2016 accelerator neutrino experiment [12].

Although it has demonstrated the sub-second time resolution and reliable time stamping necessary for imaging celestial objects, the stage-driven model is highly unsuitable for use with large aperture areas. For example, if it is used for the 10 m^2 large-area telescope that is GRAINE's future goal, it would weigh 1700 kg and thus significantly affect the weight limits of other components. Therefore, scientific observations would require a major change of model for the multi-stage shifter.

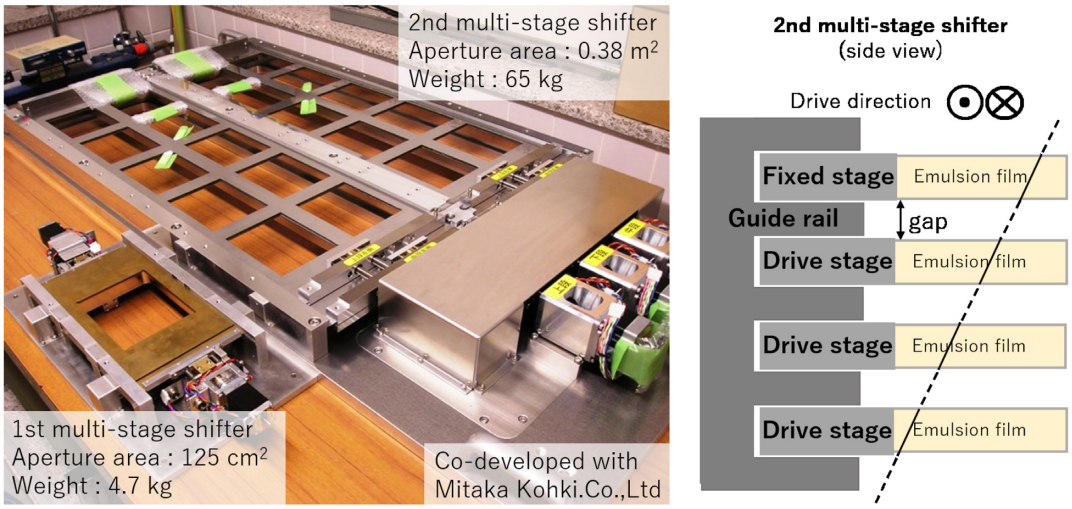

Fig. 1. The conventional multi-stage shifter model. The left-hand picture shows the first and second multi-stage shifters. The right-hand picture schematically depicts the side view. The shifter consists of a fixed stage and three drive stages that follow metal guide rails.

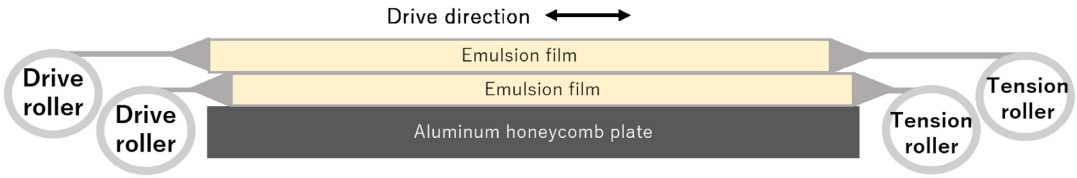

Fig. 2. Schematic depiction of the roller-driven model. Both ends of the film pack are fixed to a pair of rollers; i.e., a drive roller and a tension roller. The drive roller is connected to the motor via gears. A winding spring is built into the tension roller.

2.2 *New model*

The new shifter is a roller-driven model [16]. Both ends of its film pack are pulled by a drive roller and tension roller pair (Fig. 2); the drive roller is connected to the motor via gears. A winding spring is built into the tension roller to keep a certain tension. Eliminating stages and guide rails should significantly reduce the weight. This would allow the model to be made larger, and more positional states could be achieved by adding stages. As the film packs are in contact with each other, the gap between films is significantly reduced compared with conventional models; this improves spatial resolutions in the track (reconstruction accuracy). The resolution of arrival time (σ_t) is determined by the driving speed of the fastest moving film ($v_{fastest}$) and the reconstruction accuracy of the positional displacement of the tracks (σ_{dx}) (Eq. 1):

$$\sigma_t = \frac{\sigma_{dx}}{v_{fastest}}. \tag{1}$$

The uncertainty of the shift velocity is smaller than reconstruction accuracy. Therefore, a reduction in the gap improves the time resolution.

Figure 3 shows the first practical model of the roller-driven shifter. It has an aperture area of 1.25 m^2 and a mass of 80 kg. The weight per unit area is approximately 1/3 that of the conventional model (Table 1). It has five pairs of drive and tension rollers, and the topmost drive roller is a fixed roller without a motor.

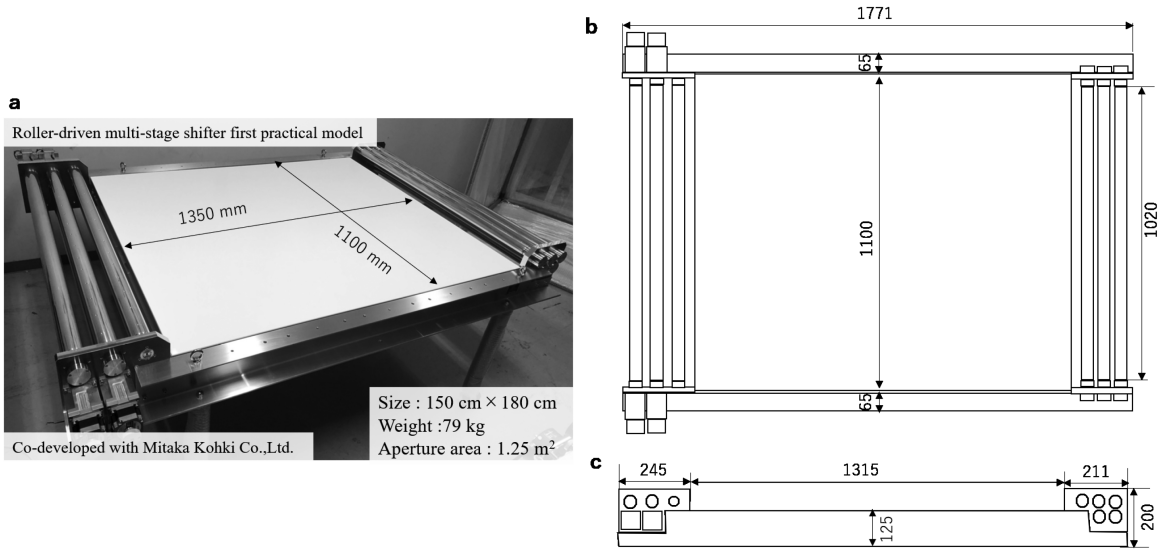

Fig. 3. (a) Photograph of the first practical model of a roller-driven shifter and diagrams of the (b) top and (c) side view. It has five pairs of drive and tension rollers, and the topmost drive roller is a fixed roller without a motor.

Table 1. Comparison of stage-driven and roller-driven models.

Model	Stage-driven	Roller-driven
Aperture area [m^2]	0.38	1.25
Mass [kg]	65	80
Mass / Aperture area [kg m^{-2}]	171	64
Number of driven stages	3	4

3. Operation testing

3.1 *Film packs*

To demonstrate that the new shifter has sufficient time resolution for balloon experiments, we evaluated the performance of the first roller-driven shifter in an operational test. We observed secondary cosmic rays (muons) using emulsion films and evaluated the shifter's time resolution. We prepared the emulsion films at Nagoya University, at the end of May 2021. The film had a base thickness of 210 μm and an emulsion thickness of 75 μm. The film pack was made on June 21, 2021, using a vacuum packaging machine.

Figure 4 shows the film pack used in this test. A highly rigid, low-mass backplate of carbon fiber reinforced plastic (CFRP) was sandwiched between polyvinyl chloride (PVC) sheets—which replaced the emulsion film—and packed with laminated sheets. One pack measured 50 cm × 125 cm, more than six times larger than the film pack used in the 2018 experiment. To make the ends of the packs rigid, 50 μm-thick stainless foil (SUS304) was used, which was thermally bonded to the laminated sheets using Fixelon ® (Aicello Co.,Ltd.). Two film packs were pulled by each roller pair, and small pieces of film (10 cm × 12.5 cm) were mounted on one side of each pack. These films were inserted into pre-cut holes in the PVC sheet on the top surface. Three pre-cut holes were located at both ends (drive side and tension side) and the center of each pack. Therefore, a total of 15 films were used.

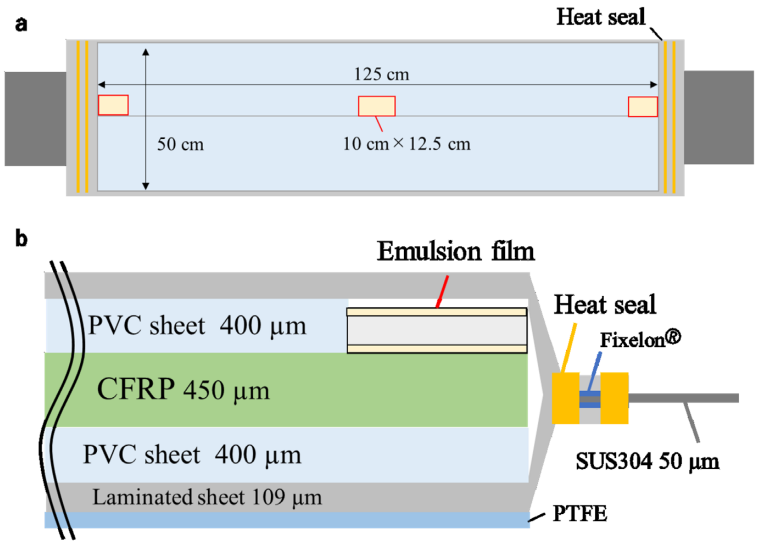

Fig. 4. Composition of film packs: (a) top and (b) side view.

Table 2. Operation details.

Operation	Waiting	Imaging operation	High-resolution operation
Time	6/22 22:35:51– 6/23 07:03:52	6/23 19:09:34– 6/24 00:17:07	6/24 12:21:52– 6/24 17:35:48
Roller1	Rest at −500 μm	200 μm per step, total 6 steps	
Roller2	Rest at 10 mm	200 μm per step and 20 steps per stroke	
Roller3	Rest at −500 μm	1.5 mm per stroke 10 μm s^{-1} continuous drive	1.35 mm per stroke 10 μm s^{-1} continuous drive
Roller4	Rest at 10 mm	Rest at 0 μm	1.5 mm per stroke 100 μm s^{-1} continuous drive

To reduce friction during driving, a 50 μm-thick polytetrafluoroethylene (PTFE) sheet with good sliding properties was inserted between the packs.

Testing started immediately after setting the film on the shifter the following day. After completing the operation test on June 24, the film packs were immediately unpacked and all films were developed the next day. In August 2021, all tracks were read using an emulsion scanning system (Hyper Track Selector, HTS [17]) at Nagoya University.

3.2 *Operation*

Table 2 lists the operations in this test. The rollers are labeled 0 (the fixed roller), 1, 2, 3 and 4 from top to bottom. To demonstrate that the roller-driven model has the same or better time resolution compared with the stage-driven model, two kinds of operation were conducted. One was *imaging operation* simulating the 2018 experiment with four pairs of rollers, which aimed for the sub-second time resolutions required for imaging objects. The other was a *high-resolution operation* with all rollers, which aimed for the 0.1 s time resolution required for 0.1° resolution imaging.

During imaging operation, rollers 1 and 2 were driven in steps of 200 μm, and roller 3 was driven continuously at 10 μm s^{-1} for 1.5 mm. The shifter made a reciprocating motion, with a period of movement in one direction defined as one stroke. The upper roller moved one step

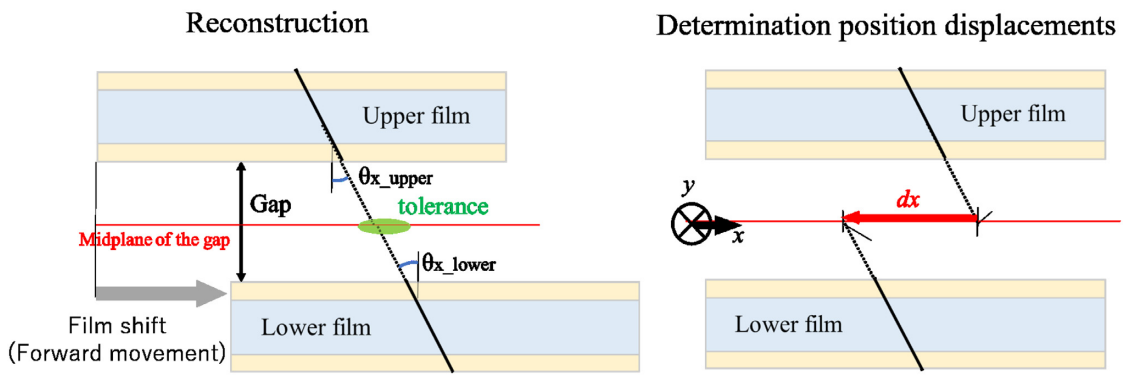

Fig. 5. Definition of position displacement. On the midplane of the gap, the position displacement is defined as (the position of the lower film track) − (the position of the upper film track), and it is represented by *dx* in the direction of film shift and *dy* vertically.

every time the lower roller finished one stroke. Position displacemant of tracks found in the second and third layers can provide 1 s time resolution with 10 μm reconstruction accuracy.

In high-resolution operation, in addition to imaging operation, roller 4 was continuously driven at 100 μm s^{-1} for 1.5 mm. In the time taken for roller 4 to go back and forth nine strokes, roller 3 finished one stroke, so roller 3's stroke was 1.35 mm. Position displacemant of tracks found in the third and forth layers can provide a 0.1 s time resolution with 10 μm reconstruction accuracy.

Before these operations, we also introduced a waiting operation, which had similar background tracks as the waiting period before launch in a balloon experiment. During this operation, each roller rested at a designated location for about eight hours.

4. Results

4.1 *Reconstruction*

After development, all 15 films were scanned by the HTS at Nagoya University. The scan area was 80 mm × 110 mm, nearly 1 cm inside the film edge. The scanned tracks were reconstructed between two films at a time by using NETSCAN. Each track was extrapolated to the midplane of the gap between films, and they are reconstructed if the deviation of the angle and position is within a certain tolerance (Fig. 5). First, we determined the alignment between two films by using tracks accumulated during the waiting operation where film positions are fixed. Starting from the design value, we adjusted the alignment by iterating such that the number of reconstructed tracks is maximized. After that, we reconstructed tracks accumulated during all operation by allowing position displacement in the direction of film shift. On the midplane, position displacement is defined as (the position of the lower film track) − (the position of the upper film track), which is represented by *dx* in the direction of film shift and *dy* in the direction perpendicular to *x* on the film plane. The direction in which the film moves forward takes a positive value, so *dx* is negative. Tracks can be classified into different time periods by using the distribution of these position displacements.

For tracks on the center of the pack, Fig. 6 shows the distribution of roller 1's position displacement relative to roller 0 during imaging operation. There are clusters at intervals of about 200 μm which correspond to the step spacing of roller 1. Therefore, tracks in each cluster were recorded during about 50 min of rest time at each step of roller 1. Each cluster was assigned to

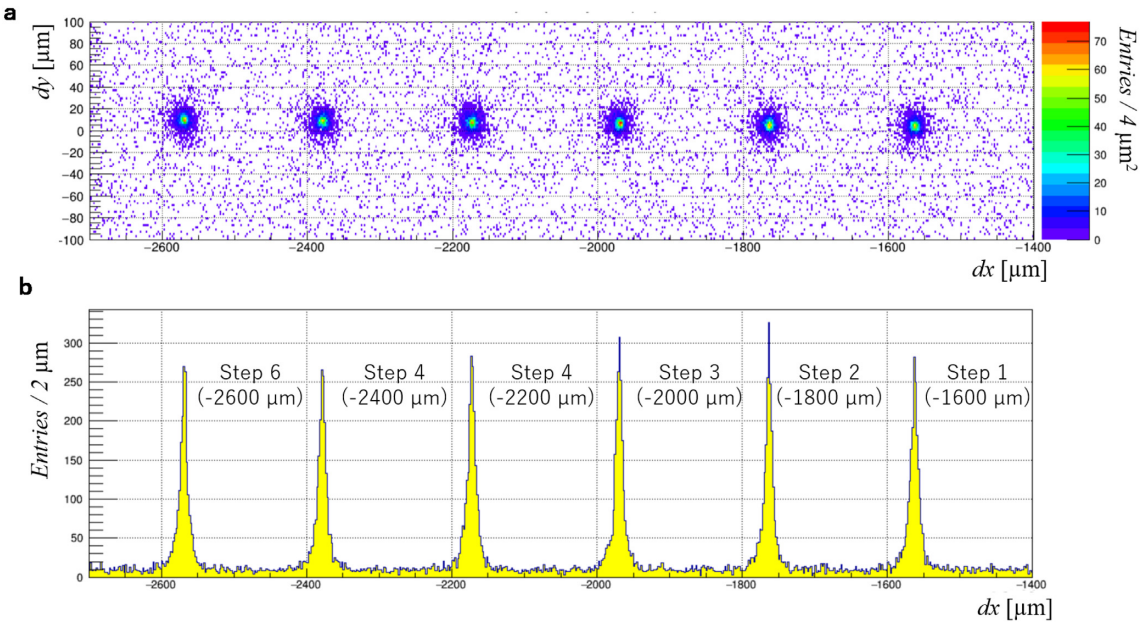

Fig. 6. Distribution of position displacement for tracks reconstructed between rollers 0 and 1 during the imaging operation. Panel (a) shows two-dimensional distribution. Panel (b) shows dx distribution. The logical position displacements in each step are shown in parentheses.

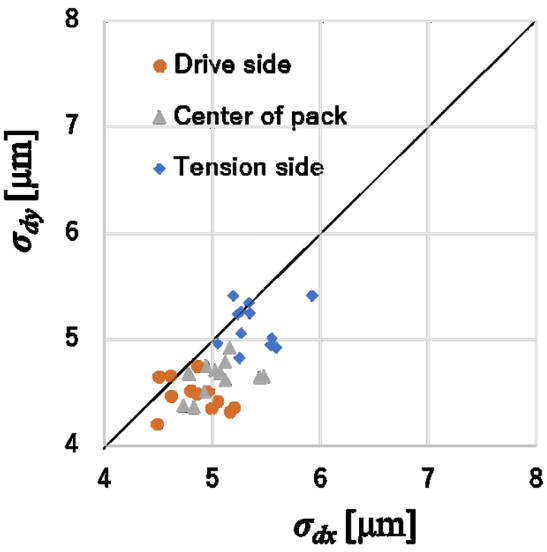

Fig. 7. Reconstruction accuracy of tracks reconstructed between rollers 0 and 1. The circles represent the drive roller, the triangles represent the center of the pack, and the diamonds represent the tension roller.

each step of roller 1 by the logical position displacements calculated from the operation. For example, the logical position of the first step during imaging operation is -1600 μm.

We then evaluated the reconstruction accuracy for each cluster. We made Gaussian fitting the dx distribution for $|\tan\theta_x| < 1.0$ and the dy distribution for $|\tan\theta_y| < 1.0$; 1σ was defined as the accuracy of the track reconstruction σ_{dx} and σ_{dy}. Figure 7 summarizes the reconstruction accuracies σ_{dx} and σ_{dy} for all 12 clusters.

All clusters obtained reconstruction accuracies within 6 μm. The reconstruction accuracy on the tension side was inferior, because the gap between films was more uneven than for the

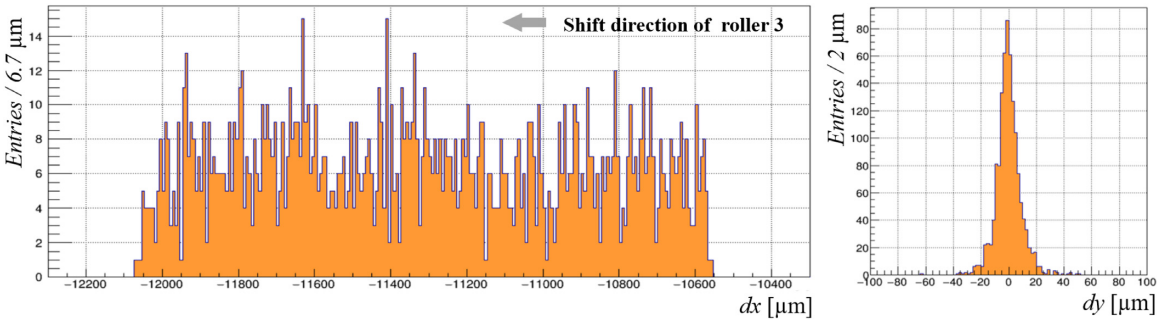

Fig. 8. Distribution of position displacement of tracks reconstructed between rollers 2 and 3 during imaging operation.

Table 3. Reconstruction accuracy σ_{dy} of tracks reconstructed between rollers 2 and 3.

Operation	Imaging operation				High-resolution operation			
Direction of roller 2	Forward		Back		Forward		Back	
Direction of roller3	Forward	Back	Forward	Back	Forward	Back	Forward	Back
σ_{dy}[μm]	7.5	7.3	7.9	7.5	7.8	7.5	7.7	7.3

others due to the film riding up on the PVC sheet. Although σ_{dx} is larger than σ_{dy} because of the direction of film shift, the difference is small, within 1 μm.

4.2 *Time resolution*

We similarly reconstructed all tracks up to roller 3 for imaging operation and up to roller 4 for high-resolution operation. For tracks on the center of a pack, Fig. 8 shows the distribution of roller 3's position displacement relative to roller 2 (at rest at step 1) during imaging operation. Only the case where rollers 2 and 3 were both in the forward movement stroke is shown. There is a banded cluster about 1.5 mm long, consistent with the continuous driving of roller 3. As dx was continuously changing, only σ_{dy} was obtained by Gaussian fitting. Table 3 lists the σ_{dy} for each operation, classified by the shift direction. All operations obtained reconstruction accuracies of $\sim$8 μm. These are worse than rollers 1 and 2 because rollers 1and 2 were at rest at each step, but roller 3 moved continuously. As roller 3 was continuously driven at 10 μm s^{-1}, the time resolution σ_t was less than 0.1 s from Eq. (1). Therefore, the roller-driven shifter demonstrated sub-second time resolution.

We also evaluated the time resolution during high-resolution operation in the same way. As roller 3 was driven continuously (unlike rollers 1 and 2), it is not easy to classify clusters according to the shift direction of roller 4. In this case, assuming that roller 3 maintained constant velocity within a stroke, the clusters were classified by division into nine equal parts.

For tracks on the center of a pack, Fig. 9 shows the distribution of roller 4's position displacement relative to roller 2 (at rest at step 1) during high-resolution operation. Only the case where rollers 3 and 4 were both in the forward stroke is shown. There is a banded cluster about 1.5 mm long. Table 4 lists σ_{dy}, classified by the shift direction. A reconstruction accuracy of 10 μm was obtained, suggesting that a 0.1 s time resolution could be achieved. However, the distribution in Fig. 9 shows a peak where the tracks were concentrated at the left-hand end of the cluster. This was because the film was stagnant due to gear backlash during the turnaround.

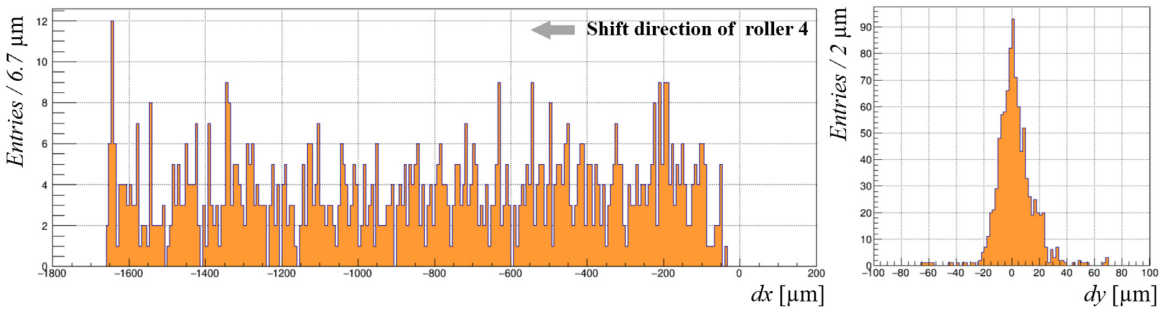

Fig. 9. Distribution of position displacement of tracks reconstructed between rollers 2 and 4 during high-resolution operation.

Table 4. Reconstruction accuracy σ_{dy} of tracks reconstructed between rollers 3 and 4 during high-resolution observation.

Direction of roller 2	Forward				Back			
Direction of roller 3	Forward		Back		Forward		Back	
Direction of roller 4	Forward	Back	Forward	Back	Forward	Back	Forward	Back
σ_{dy} [μm]	9.4	7.4	8.7	8.7	10.1	8.7	8.3	8.1

It is also possible that the constant velocity of roller 3 was disrupted at that time, which prevented correct cluster classification. The tracks during roller 4's back stroke may consequently be mixed with those in the forward stroke. Therefore, it is necessary to design the operation so that the start point of the 1.5 mm continuous stroke does not overlap with the turnaround area.

4.3 *Gap between films*

In the new shifter, the film packs were in contact with each other, so the gap between the films was significantly reduced compared with that in conventional models. We evaluated the deviation of the actual gap from the design value using the tracks during the waiting operation. For each pair of upper and lower film tracks that can be reconstructed, the true gap between films can be determined from the position and angle of each track. As the film was mounted only on the upper side of the film pack in this test, the designed gap between films is 1158 μm.

Figure 10 shows the difference dz between the true gap and the design value, where dz is defiend by (true gap) − (design value). Other than between rollers 3 and 4, dz was within 100 μm and close to the design value. It was not normally distributed due to asymmetric boundary conditions such as packs touching each other. The gap between rollers 3 and 4 was larger than the others and was non-uniform, because the corner of roller 4's film was riding up on the PVC. This occurred owing to the use of small films, and so could be avoided by using large films for the balloon experiment (25 cm × 125 cm).

In the next balloon experiment, they will be mounted on both sides of the film pack, but in this operational test films were mounted only on the upper side. Based on the results of this test, we estimated the gap in the next balloon experiment. Table 5 compares the estimation with typical values for the conventional model, showing that the gap can be reduced by more than half. The relationship between the gap and reconstruction accuracy is expressed by the following equation, where l is half of the gap between films.

$$\sigma_{dx} = \sqrt{2}\sqrt{(\sigma_x)^2 + 2(\tan\theta_x \cdot \sigma_l)^2 + l^2(\sigma_{\tan\theta_x})^2} \tag{2}$$

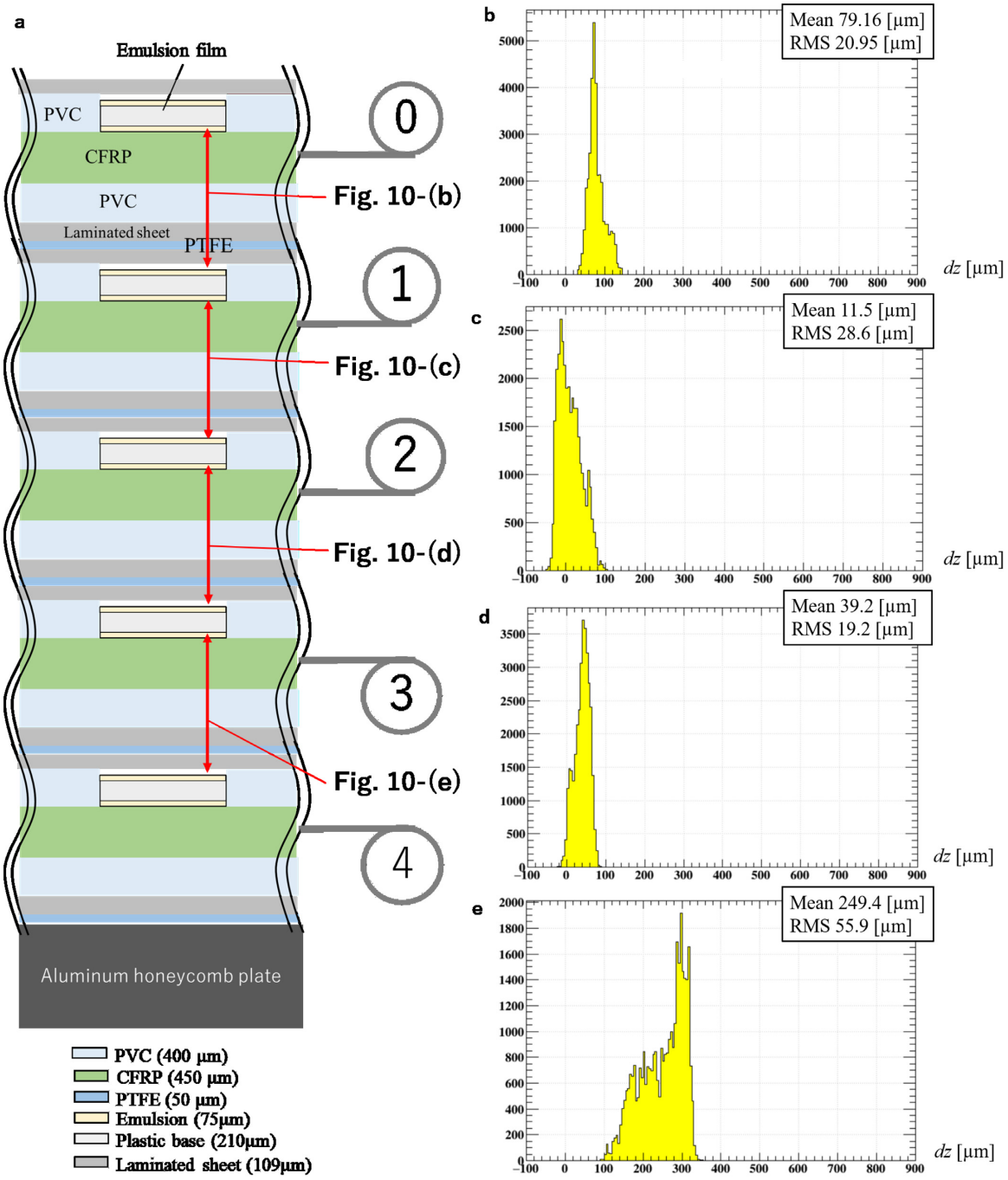

Fig. 10. Deviation from the design value (1158 μm) of the gap between films obtained from reconstruction. Panel (a) shows the side view of each gap. The histograms on the right show true gaps between (b) rollers 0 and 1, (c) rollers 1 and 2, (d) rollers 2 and 3, and (d) rollers 3 and 4.

Table 5. Gaps in conventional model and roller model.

Between	Conventional model [μm]	Roller model [μm]
Stage/roller 0 and stage/roller 1	900 $\pm$ 50	347 $\pm$ 21
Stage/roller 1 and stage/roller 2	900 $\pm$ 50	307 $\pm$ 19
Stage/roller 2 and stage/roller 3	600 $\pm$ 140	279 $\pm$ 29
Roller 3 and roller 4	–	567 $\pm$ 56

Although σ_x and $\sigma_{tan\theta_x}$ are derived from the reading error of the HTS, σ_x and $\tan\theta_x \cdot \sigma_l$ are clearly smaller than $l \cdot \sigma_{\tan\theta_x}$. Therefore, the reduction of gaps significantly improves the reconstruction accuracy. For example, between rollers 0 and 1, an almost three-fold improvement can be expected. As the reconstruction accuracy directly improves the time resolution, as expressed in Eq. 1, the acquisition of a time resolution of tens of milliseconds is also feasible. Therefore, the introduction of the new shifter will enable high-resolution imaging of gamma-ray sources as well as phase-resolved analysis of pulsars.

5. Conclusion

By changing the drive mechanism from the conventional model, the roller-driven model is 1/3 lighter per unit area, allowing it to have a large aperture area; the lighter structure also enables longer observations by adding more layers. Operation testing with emulsion films (10 cm × 12.5 cm) suggested this model can achieve sub-second time resolution equivalent to the 2018 experiment. We also showed that the gap between films is reduced by more than half compared with the conventional model and demonstrated the possibility of improving the reconstruction accuracy by nearly three times. In addition, by adding a layer which move at 100 μm s^{-1}, we can acquire a time resolution of tens of milliseconds. Overall, the roller-driven model enables large-area observations with emulsion telescopes for long durations and at high time resolution. This model can achieve 0.1° astronomical imaging of gamma-rays above 1 GeV and 0.1 s time resolution to allow measurement of the time phases of gamma-rays arriving from pulsars.

We aim to prepare the multi-stage shifter for balloon experiments in 2023 by conducting operational tests at low temperatures and low pressure among other preparatory works.

Acknowledgment

We appreciate the support provided by the F-laboratory at Nagoya University. We also thank Mitaka Kohki Co.,Ltd. for codevelopment of the multi-stage shifter and Aicello Co.,Ltd. for supplying of Fixelon®. This work was supported by JSPS KAKENHI (grant numbers 26247039, 26800138, 17H06132, 18H01228, 21H04472, and 21J20707).

References

[1] S. Aoki et al. Nucl. Instrum. Meth. B **51**, 466 (1990).
[2] K. Morishima and T. Nakano, J. Instrum. **5**, P04011 (2010).
[3] K. Kodama et al. Nucl. Instrum. Meth. A **493**, 45 (2002).
[4] S. Takahashi et al. Nucl. Instrum. Meth. A **620**, 192 (2010).
[5] S. Takahashi, et al., Prog. Theor. Exp. Phys. **2015** 043H01 (2015).
[6] H. Rokujo et al. Nucl. Instrum. Meth. A **701**, 127 (2013).
[7] S. Takahashi, et al., Prog. Theor. Exp. Phys., **2016** 073F01 (2016).
[8] F. Mizutani et al., Aerospace Tech. Japan **16**, 6 (2018).
[9] S. Takahashi, et al., Prog. Theor. Exp. Phys. submitted , (2021).
[10] K. Yamada et al., Prog. Theor. Exp. Phys. **2017**,063H02 (2017).
[11] T. Fukuda, et al., Prog. Theor. Exp. Phys. **2017** 063C02 (2017).
[12] H. Oshima, et al., Prog. Theor. Exp. Phys. **2021** 033C01 (2021).
[13] S. Aoki et al., Nucl. Phys. B Proc.Suppl. **196**, 50 (2009).
[14] K. Ozaki, S. Takahashi, S. Aoki, K. Kamada, T. Kaneyama, R. Nakagawa, and H. Rokujo, Nucl. Instr. Meth. A **833**, 165 (2016).
[15] W. B. Atwood et al. Astrophys. J. **697**, 1071 (2009).
[16] S. Takahashi et al., Adv. Space Res. **62**, 2945 (2018).
[17] M. Yoshimoto, et al., Prog. Theor. Exp. Phys. **2017** 103H01 (2017).